UWB MIMO Slot Antenna with Minkowski Fractal Shaped Isolators for Isolation Enhancement

Paramita Debnath[2], Anirban Karmakar[2, *], Anuradha Saha[1], and Shabana Huda[3]

Abstract—A novel compact ultra-wideband (UWB) multiple input multiple output (MIMO) slot antenna with band notch characteristics is presented for portable wireless UWB applications. The antenna comprises co-planar waveguide feed (CPW) and two radiating monopoles oriented in orthogonal orientation for providing orthogonal radiation patterns. A Minkowski fractal parasitic stub along with a Minkowski fractal grounded stub has been placed at 45° between the monopoles to reduce the coupling between them which in turn establish high isolation between the radiators. An excellent band notch characteristic is obtained at 5.5 GHz by etching a modified E-shaped compact slot on the radiators. At the centre of notched band, the efficiency and gain of the antenna drop significantly which indicates a good interference suppression. Results show that the designed antenna meets −10 dB impedance bandwidth and −17 dB isolation throughout the entire operating band (3.1–12 GHz). Novelty of this design lies in improving isolation using compact fractal structures which occupy less space than conventional isolation mechanisms in MIMO structures. The simulated and measured results show that the proposed antenna is convenient for MIMO diversity systems.

1. INTRODUCTION

Ultra-wideband (UWB) is an extremely trending technology in modern communication systems for providing high data rate and reliable communication. In February 2002, the Federal Communication Commission (FCC) allocated a bandwidth of 7.5 GHz (3.1 GHz to 10.6 GHz) for UWB [1]. Since then, the UWB technology has been rapidly advancing and leading to innovations, and has attracted much attention. Conventional UWB technologies face challenges such as multipath fading and high bit error rate [2]. To resolve this limitation, multiple-input multiple-output (MIMO) technology has been evolved [3]. MIMO employs multiple antennas at the transmitting and receiving ends for improving the data rate and quality of communication without utilization of additional power [3]. Designing a compact planar MIMO antenna with high isolation operating over the entire UWB bandwidth is a growing challenge nowadays. One should also ensure that the isolation improvement mechanism should not influence the wideband impedance characteristics of the proposed antenna. Some of the commonly used techniques for suppressing mutual coupling are diversity techniques [4] which are already reported as decoupling structures such as tree like structures [5], parasitic meander-lines [6] and inserting stubs [7]. The UWB spectrum consists of several pre-assigned (by FCC) narrow bands, and some of them are Wi-Max (3.3–3.7 GHz) and IEEE 802.11 wireless local area network (WLAN) operating at 5.15 GHz to 5.85 GHz, which may cause possible electromagnetic interference to UWB applications. Hence, antennas are required to filter out the undesired bands. To acquire this, several band notching techniques are proposed which include inserting T-shaped strips [8], electromagnetic band gap (EBG) structures [9],

split-ring resonators (SRR's) [10], and many more. In this design, a band notch characteristic at 5.5 GHz has been achieved by etching a modified E-shaped slot on orthogonal radiators.

In this communication, a compact band notched UWB diversity antenna is proposed which consists of CPW feed radiating planar monopoles placed at orthogonal orientation. A Minkowski fractal [11] shaped parasitic element is used in this endeavour to reduce the coupling between antenna elements. A rectangular stub with a Minkowski fractal shaped top is placed at 45° between the CPWs to establish and ensure high isolation. The impedance matching at the UWB spectrum is achieved by using conventional half circular slots on top of the radiating monopoles and by employing stepped impedance transformers. An excellent band notch characteristic has been obtained at 5.5 GHz by cutting a modified E-shaped slot on the radiating monopoles. The notch band reduces the electromagnetic interference occurring at the WLAN band (5.15–5.85 GHz). The radiation patterns and ECC show that the antenna is suitable for MIMO/diversity systems.

2. ANTENNA DESIGN

2.1. Antenna Configuration

The geometry of the proposed UWB MIMO antenna is shown in Fig. 1. The antenna is fabricated on a low cost FR4 substrate, with a relative dielectric constant 4.4, thickness 0.8 mm and loss tangent 0.02. The total dimension of the antenna is $46 \times 46 \times 0.8$ ($L \times W \times h$) mm^3. The proposed antenna comprises two orthogonal planar monopoles, a partial ground plane, a parasitic Minkowski fractal element and a grounded rectangular stub with a Minkowski fractal top. Both the monopoles are fed by a pair of co-planar waveguide (CPW) feeds as shown in Fig. 1.
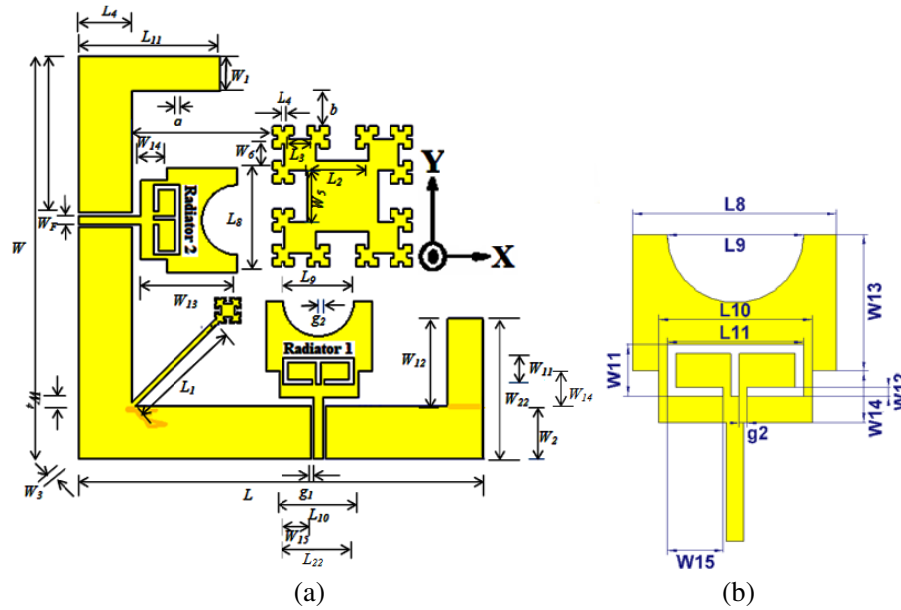
Figure 1. Schematic view of (a) the UWB MIMO antenna, (b) monopole with modified-E shaped slot.

The Minkowski fractal shaped parasitic element creates dissipative coupling to reduce mutual coupling and a rectangular stub extended from the ground plane symmetrically with respect to the ground plane at 45° to extend the effective current route which in turn enhances the wideband isolation. Each radiator has a modified E-shaped slot etched on it which provides band rejection characteristics along with compactness of notch structure as shown in Fig. 1(b). To obtain the required numerical analysis and proper geometrical dimensions, Computer Simulation Technology (CST Microwave Studio^{TM}) electromagnetic software has been exploited.

2.2. Fractal Structures for Isolation Enhancement

Application of fractal geometry on antenna optimizes the shape of antenna so as to increase the electrical path length and reduce the size of the overall radiator [11, 12]. In this MIMO configuration, a parasitic Minkowski fractal structure has been employed, which creates a dissipative coupling to cancel mutual coupling between antennas and aids in enhancing the antenna performance. As the separation of the monopoles is small, the space wave and surface wave result in coupling enhancement between them. The introduced Minkowski fractal parasitic element captures these waves and converts them into surface current resulting in reduced mutual coupling [13, 14]. When the 1st monopole is excited, due to small separation, current is coupled to the second monopole in absence of any isolation element. The presence of fractal parasitic element introduces two coupling paths between the monopoles. One is the coupling path from the 1st monopole to parasitic element, and the other coupling path is from fractal parasitic element to the second monopole. As the parasitic element is a fractal, it captures most of the energy in its elongated fractal path which in turn weakens coupled current component from the 1st monopole to 2nd monopole. The geometrical construction of fractal Minkowski curve is shown in Fig. 2 where each side of the basic structure is divided into three equal line segments, and the middle line segment of each side is replaced by an inward projection with two vertical and two horizontal line segments of equal length. This process is repeated for successive iterations while maintaining the basic geometry of the antenna [11]. Minkowski fractal algorithm (MFA) [15] using IFS for creating the scaled down copies of the original geometry is described below. The MFA can be implemented by three parameters as shown in Fig. 2(a). Here, 'a' is the length of the generator, 'b' the indentation width, and 'h' the fractal or indentation depth. Figs. 2(b)–(e) show the first four iterations of Minkowski fractal [15]. The structure is obtained starting with a square patch (or initiator). Minkowski fractal geometry is used to increase the effective current path length from 'a' to '$a + 2h$', thereby increasing electrical path length for a given frequency. The perimeter of the Minkowski fractal after the nth iteration can be found from Eq. (1) [15], as mentioned below:

$$L_{perimeter}^n = (1 + 2a_2) L_{perimeter}^{n-1} \qquad (1)$$

The area of the isolation elements after first and second iteration is found from Eqs. (3) and (4) respectively [15],

$$A^1 = (1 - 4a_1 a_2) L_o^2 \qquad (2)$$
$$A^2 = [1 - 2a_1 a_2 (3 + 3a_1^2 - 2a_1 + 4a_2^2)]L_o^2 \qquad (3)$$

where, $a_1 = \frac{b}{a}$ and $a_2 = \frac{h}{a}$.

To further intensify the isolation process, a grounded rectangular stub has been inserted and extended at 45° with respect to CPW feed to further enhance the isolation of the overall system. In this structure, a Minkowski fractal shaped top has been added to the stub which provides high isolation along with increasing stages of iterations. When grounded fractal stub is introduced, more

(a) Generator

(b) Initiator (c) 1st Iteration (d) 2nd Iteration (e) 3rd Iteration
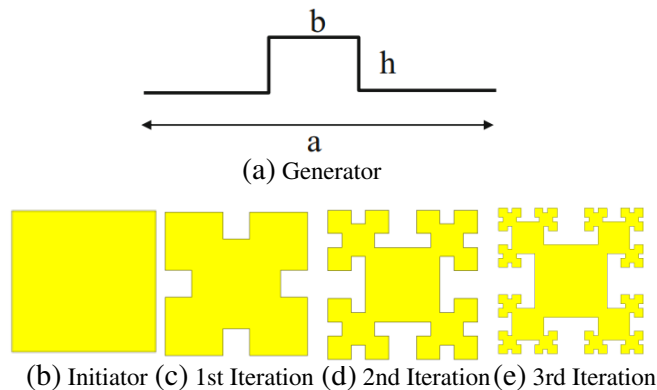
Figure 2. Recursive generation of Minkowski fractal structure.
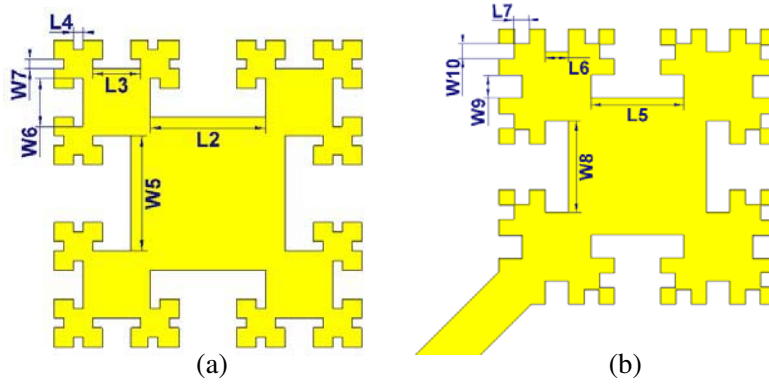
Figure 3. (a) Parasitic Minkowski fractal element, (b) Minkowski fractal stub extended at 45° from the antenna structure.

current through L-shaped ground concentrates on the grounded stub and is captured in the fractal top due to their larger electrical length. Parasitic fractal element and grounded fractal stub are shown in Fig. 3.

2.3. Modified E-Shaped Slot for Band Notch Characteristics

The UWB spectrum is severely interfered by several preassigned narrow band systems such as Wi-Max (3.3 GHz–3.7 GHz) and WLAN (5.15 GHz–5.85 GHz). The coexistence of these narrow bands may cause possible electromagnetic interference to the UWB applications. To solve this issue, modified E-shaped slot has been designed and implemented over the planar monopoles as shown in Fig. 1(b). This modified E-shape has been specially considered as it will occupy lesser space than a Euclidian notch [22]. Each slot etched on the radiators acts as a quarter (guided) wavelength parallel open circuit transmission line that shorts the antenna at a relevant notch frequency. The total length of this E-shape slot is about half wavelength of the centre frequency of the notch band which can be calculated by Eq. (4) [16]:

$$S = \frac{c}{2 f_{notch} \sqrt{\varepsilon_{eff}}} \approx 3 \cdot W_{11} + 2 \cdot L_{11} - 2 \cdot g_2 \tag{4}$$

Here, the effective dielectric constant (ε_{eff}) can be approximated to half of the dielectric constant of the FR4 material, due to the lack of ground plane. c is the speed of light, f_{notch} the centre frequency of the notch band, and S the total length of the E-shaped slot. W_{11}, L_{11}, g_2 and L_{22} are the essential design parameters as shown in Fig. 1(b). According to Eq. (5), the calculated length of the slot is 20 mm, which is close to our designed value of 23 mm.

3. RESULTS AND DISCUSSION

3.1. Impedance Characteristics

The simulated S-parameter of the antenna is shown in Fig. 4 which shows that the proposed contribution has an impedance bandwidth ($S_{11} < -10$ dB) ranging from 3.1 to 12 GHz except the WLAN (5.15 GHz–5.85 GHz) which is a notch band. Band notching at this frequency has been achieved by etching a compact E-shaped slot on both the radiators.

It is seen from Fig. 4 that adding a fractal stub for enhancing isolation has negligible effect on the wideband impedance matching of the UWB MIMO monopole. The proposed MIMO antenna has been successfully fabricated and followed by measurement using a Rhode and Schwarz ZVA-40 vector network analyzer (VNA). While measuring return loss, port-1 is excited and the other port terminated with 50 Ω load. Here port-1 is designated as the port connected with radiator-1 as shown in Fig. 1(a). The measured and simulated S-parameters are in good agreement as shown in Fig. 5 along with antenna prototype shown as an inset. The proposed UWB MIMO antenna covers the entire UWB bandwidth showing satisfactory notch characteristics at WLAN band.

Mutual coupling between neighbouring radiating monopoles in the diversity antenna introduces unwanted disturbances in the radiation pattern due to the introduction of surface waves. So, there is a requirement for additional isolation mechanism especially where strong surface current on the ground plane may be the main cause of coupling of electromagnetic energy between monopoles. In the previous section it is clear that by inserting Minkowski fractal isolation stub and parasitic fractal element, most of the current between two radiators has been trapped. This helps to reduce the mutual coupling between the adjacent antenna elements. It is evident from the parametric study as shown in Fig. 6 that the value of S_{21} is reduced to less than $-17\,\text{dB}$ for most of the operating band after the application of fractal stub along with parasitic fractal structure up to the 3rd iteration. It can be easily inferred from Fig. 6 that as the number of iterations of both the fractal structures increases, S_{12}/S_{21} characteristics decrease significantly with increasing isolation. This is for the intricacy of fractal structures which can confine more energy on them due to their larger electrical length than a Euclidian structure. The effectiveness of fractal isolators is that the isolation enhancement can be done with increasing order fractal iterations that will not occupy additional space in the radiator. We have limited this optimization up to the 3rd iteration of fractal as higher iterations may complicate the fabrication process.

Figure 7 presents the parametric variation of S_{11} characteristics for the E-shaped slot. It is seen that with the increase of the length of the slot, the centre frequency of the notch band shifts towards lower end of the operating band which in turn proves tuneable characteristics of the notch. Notch length of 23 mm is chosen as it suites the suitable notch characteristics at 5.5 GHz. Final optimized dimension of the proposed antenna is described in Table 1.
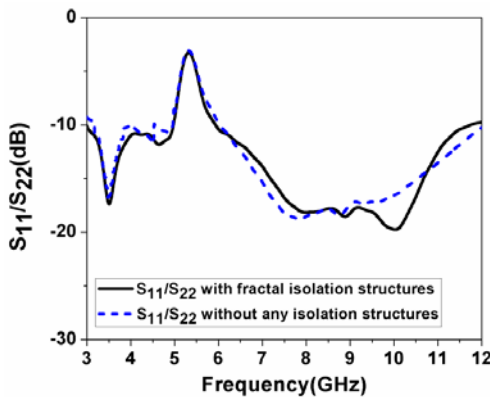
Figure 4. Simulated S_{11}/S_{22} parameter with and without isolation structures.
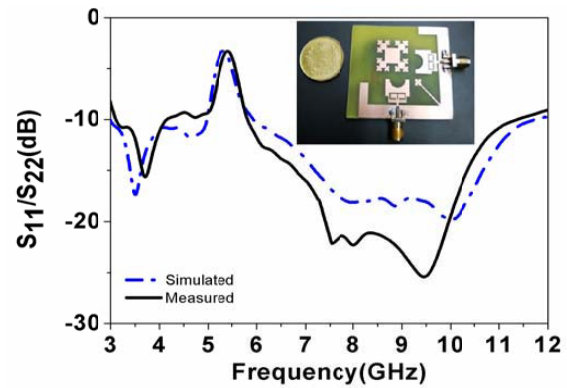
Figure 5. Simulated and measured S_{11}/S_{22} of the proposed antenna with fabricated prototype shown as an inset.
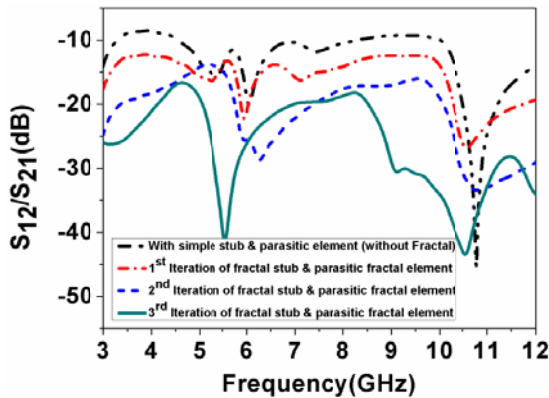
Figure 6. Simulated S_{12}/S_{21} characteristics based upon four iterations of fractal stub and parasitic fractal element.
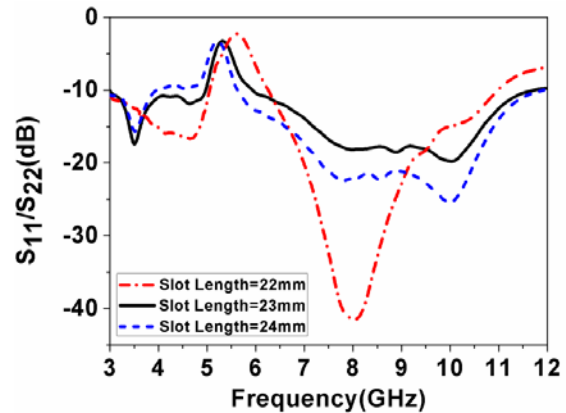
Figure 7. Simulated S_{11}/S_{22} of proposed antenna with different length of the E-shaped slot from antenna edge.

Table 1. Dimensions of the proposed antenna (Unit: mm).

Parameters	W	W_1	W_2	W_3	W_4	W_5	W_6	W_7
Unit (mm)	46	4	6	0.5	1	6	2.5	0.5
Parameters	W_8	W_9	W_{10}	W_{11}	W_{12}	W_{13}	W_{14}	W_F
Unit (mm)	1	0.25	0.16	3	0.5	8	3	1
Parameters	a	b	g_1	g_2	L	L_1	L_2	L_3
Unit (mm)	16	4	0.3	0.45	46	13.38	6	2.5
Parameters	L_4	L_5	L_6	L_7	L_8	$L_9 = L_{22}$	L_{10}	$L_{11} = W_{22}$
Unit (mm)	0.5	1	0.25	0.16	12	8	9	8

3.2. Surface Current Distribution

To elaborately express the influence of the Minkowski fractal stub and Minkowski fractal parasitic elements, the simulated surface current distribution at three different frequencies are carried out in Fig. 8. Fig. 8(a) shows the UWB MIMO antenna with and without fractal stub at a lower edge frequency of 4 GHz, where port 1 is excited and port 2 terminated at 50 Ω impedance. It can be seen that without the fractal stub and parasitic element, strong current is coupled from one port to another by direct current through common ground plane as well as induced current through radiating monopoles which may result in high mutual coupling. When grounded fractal stub and fractal parasitic element are introduced, more current through ground concentrates on the grounded stub and is captured in the fractal. Side by side, induced current through radiating monopoles is also captured by the parasitic element and concentrated on the fractal which in turn reduces the mutual coupling. The same effect can be seen at higher frequency of 7.5 GHz as shown in Fig. 8(c). Thus, the fractal stub in combination with parasitic element causes high isolation (-17 dB) between the two ports which is higher than other reported works [5, 8, 9, 11, 13, 16, 18–21, 23–26]. Also the antenna has larger impedance bandwidth than [5, 11, 16, 20–26]. At the notch frequency of 5.5 GHz as shown in Fig. 8(b), the current is concentrated around the E-shaped slots absorbing radiative energy making the antenna non-radiative on that specific frequency, where the band-notching characteristics are obviously produced. Novelty of this structure lies in achieving comparatively higher isolation using novel fractal shape isolators where the isolation is higher than earlier reported works.

4. DIVERSITY CHARACTERISTICS:

One of the primary requirements for diversity antenna elements to be effectively deployed in pattern diversity is that their radiation patterns should be uncorrelated. The mutual coupling between adjacent antenna elements and the amount of correlation between each antenna can be studied in terms of envelope correlation coefficient (ECC); the ECC can be calculated using S-parameters [17]:

$$ECC = \frac{|S_{11}^* S_{12} + S_{21}^* S_{22}|^2}{\left(1 - |S_{11}|^2 - |S_{21}|^2\right)\left(1 - |S_{22}|^2 - |S_{12}|^2\right)} \tag{5}$$

Under normal operating conditions, the value of ECC should be less than 0.5 that depicts acceptable limit of signal distortion [17]. It can be observed from Fig. 9 that due to the effectiveness of the proposed antenna (with fractal isolation structures) the simulated ECC is less than 0.02 throughout the operating bandwidth. The obtained value of ECC is well underneath the pragmatic threshold value of 0.5. For these UWB antennas, the variation of Group Delay is within 1 ns for the whole operating band. For measurement, two identical antennas have been placed at 12 cm apart, and group delay is measured with the performance network analyzer.

The simulated and measured peak gains and radiation efficiencies of the antenna (with port 1 excited) are shown in Figs. 10(a) & (b) throughout the operating band. It can be seen that except the
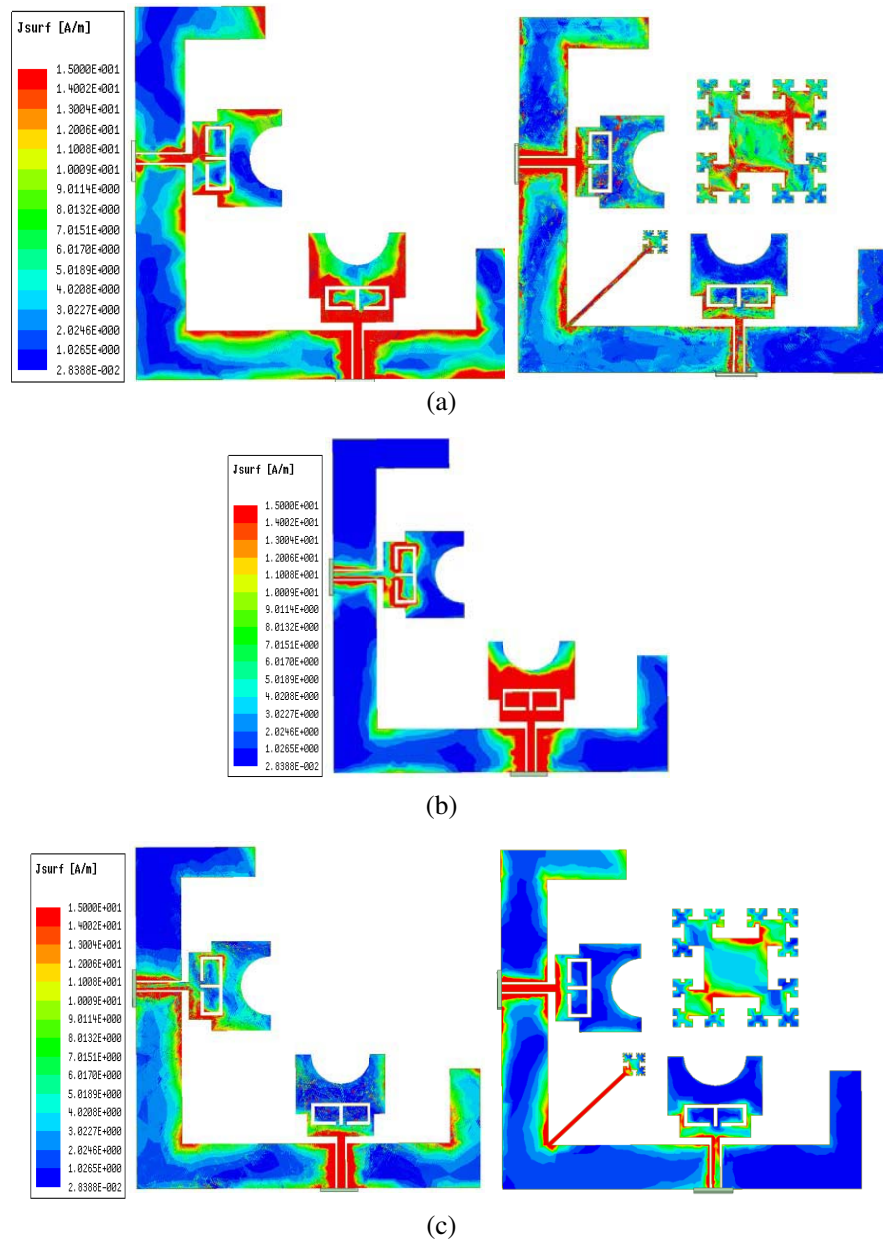
Figure 8. Simulated surface current distribution with and without fractal stub and parasitic fractal element at (a) 4 GHz, (b) 5.5 GHz, (c) 7.5 GHz where port-1 is excited and port-2 is terminated by 50 termination.

notch band of 5.5 GHz the measured peak gain ranges from 3 to 5 dBi across the entire UWB spectrum with a radiation efficiency of $> 75\%$.

A sharp decreasing trend is clearly observed at 5.5 GHz for both plots, which demonstrate the effective notch characteristics at WLAN band. It is clearly observed that except the notch band, the gain and radiation efficiencies are nearly stable across the entire UWB bandwidth. The radiation patterns of the normalized gain of the MIMO antenna have been simulated and measured with port-2 terminated with 50 ohm termination and port-1 excited, shown in Fig. 11. The proposed antenna shows a nearly omnidirectional radiation pattern over the desired operating band. Nearly omnidirectional patterns have been observed in the H-plane which is typical for monopole antennas.

Radiation patterns in E-plane are not dumbbell shaped and do not have significant null which may
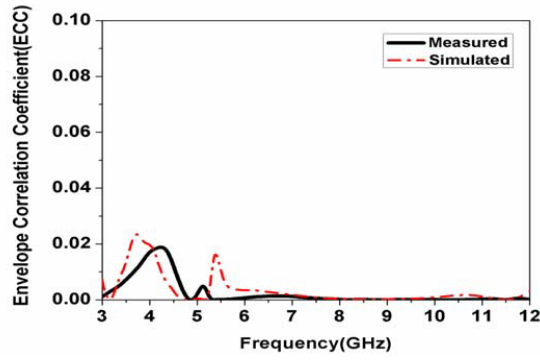
Figure 9. Simulated and measured ECC of the proposed antenna.
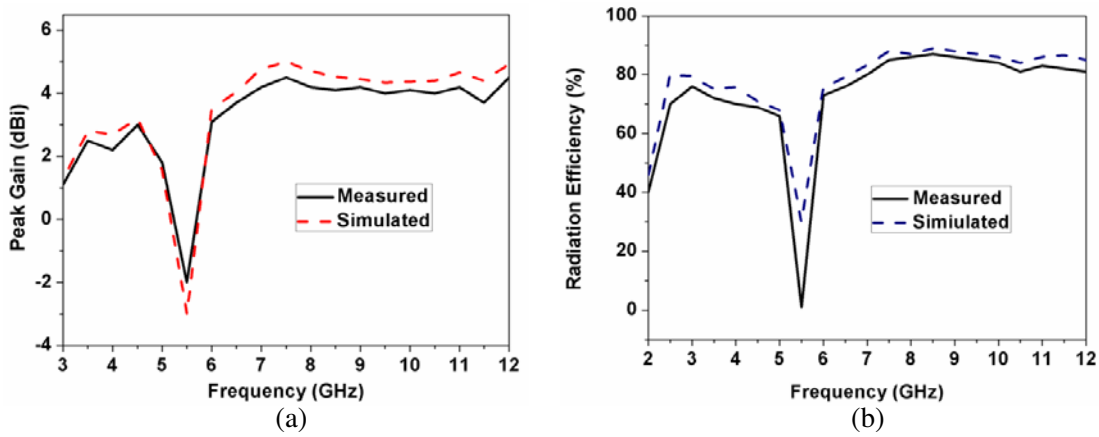
Figure 10. Simulated and measured (a) gain, (b) radiation efficiency of the proposed antenna (Port 1 excited).
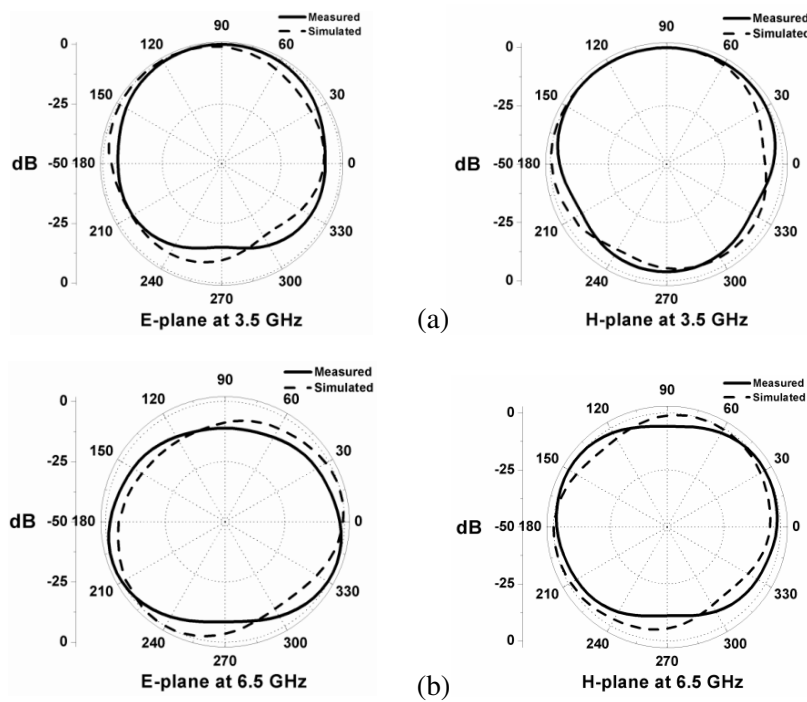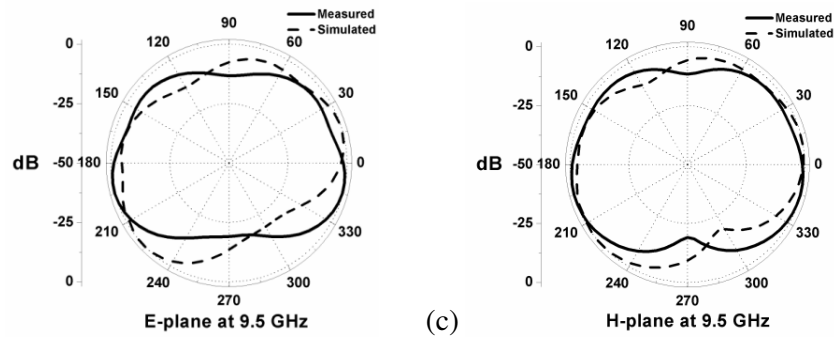
Figure 11. Radiation patterns of the proposed antenna (Port-1 excited and Port-2 terminated with 50 ohm termination).

be different from this kind of typical single monopole antennas caused for the L-shaped ground plane that makes the current distribution different from typical monopole antennas. At higher frequencies, radiation patterns are less omnidirectional due to higher order modes.

5. CONCLUSION

A compact printed band-notched UWB MIMO antenna with high isolation and band notch characteristics has been presented and analysed for portable UWB applications. The proposed antenna has an operational impedance bandwidth of $S_{11} \leq -10\,\text{dB}$ ranging from 3.1 to 12 GHz excluding a rejection band centred at 5.5 GHz. The numerical and empirical results show good resemblance. The results have also depicted that the proposed antenna has high isolation of $> 17\,\text{dB}$ over the entire UWB operational bandwidth. The overall footprint of the antenna may be comparatively large, but the focus of this design improves isolation between the antenna elements using novel and compact fractal shaped isolators without taking any additional space in MIMO structure. The ECC (Envelope Correlation Coefficient) is less than 0.002 for the entire UWB spectrum with an average realized gain of 4 dBi and radiation efficiency greater than 75% throughout the operating bandwidth making it an exceptional candidate for various UWB MIMO wireless systems.

REFERENCES

1. Federal Communications Commission, Washington, DC, USA, "Federal communications commission revision of Part 15 of the Commission's rules regarding ultra-wideband transmission system from 3.1 to 10.6 GHz," 98–153, ET-Docket, 2002.
2. Jensen, M. A. and J. W. Wallace, "A review of antennas and propagation for MIMO wireless communication," *IEEE Trans. Antennas Propag.*, Vol. 52, No. 11, 2810–24, 2004.
3. Kaiser, T., F. Zheng, and E. Dimitrov, "An overview of ultra-wide-band systems with MIMO," *Proc. IEEE*, Vol. 97, No. 2, 285–312, 2009.
4. Zhang, S., B. K. Lau, A. Sunesson, and S. He, "Closely-packed UWB MIMO/diversity antenna with different patterns and polarizations for USB dongle applications," *IEEE Trans. Antennas Propag.*, Vol. 60, No. 9, 4372–4380, 2012.
5. Zhang, S., Z. Ying, J. Xiong, and S. He, "Ultrawideband MIMO/diversity antennas with a tree-like structure to enhance wideband isolation," *IEEE Antennas Wireless Propag. Lett.*, Vol. 8, 1279–1282, 2009.
6. Iqbal, A., O. A. Saraereh, A. W. Ahmad, and S. Bashir, "Mutual coupling reduction using F-shaped stubs in UWB-MIMO antenna," *IEEE Access.*, Vol. 6, 2755–2759, 2018.
7. Ghosh, J., S. Ghosal, D. Mitra, and S. R. BBhadra Chaudhuri, "Mutual coupling reduction between closely placed microstrip patch antenna using meander line resonator," *Progress In Electromagnetics Research Letters*, Vol. 59, 115–122, 2016.

8. Gallo, M., et al., "A broadband pattern diversity annular slot antenna," *IEEE Trans. Antennas Propag.*, Vol. 60, No. 3, 1596–1600, 2012.

9. Li, Q., A. P. Feresidis, M. Mavridou, and P. S. Hall, "Miniaturized double-layer EBG structures for broadband mutual coupling reduction between UWB monopoles," *IEEE Trans. Antennas Propag.*, Vol. 63, No. 3, 1168–1171, 2015.

10. Li, L., Z. L. Zhou, J. S. Hong, and B. Z. Wang, "Compact dual-band-notched UWB planar monopole antenna with modified SRR," *Electron. Lett.*, Vol. 47, No. 17, 950–951, 2011.

11. Choukiker, Y. K., S. K. Sharma, and S. K. Behera, "Hybrid Fractal shape planar monopole antenna covering multiband wireless communications with MIMO implementation for handheld mobile devices," *IEEE Trans. Antennas Propag.*, Vol. 62, No. 3, 1483–1488, 2014.

12. Abed, A. T., "Highly compact size serpentine-shaped multiple-input-multiple-output fractal antenna with CP diversity," *IET Microwaves, Antennas & Propagation*, Vol. 12, No. 4, 636–640, 2018.

13. Khan, B. D. B. M. S., A. D. Capobianco, M. F. Shafique, B. Ijaz, and A. Naqvi, "Isolation enhancement of a wideband MIMO antenna using floating parasitic elements," *Microwave and Optical Technology Letters*, Vol. 57, No. 7, 1677–1682, 2015.

14. Li, Z., Z. Du, M. Takahashi, K. Saito, and K. Ito, "Reducing mutual coupling of MIMO antennas with parasitic elements for mobile terminals," *IEEE Trans. Antennas Propag.*, Vol. 60, No. 2, 473–481, 2012.

15. Kumar, M. and V. Nath, "Introducing multiband and wideband microstrip patch antennas using fractal geometries: Development in Last Decade," *Science Business Media. Wireless Pers. Commun.*, 1–27, Springer, LLC, 2017.

16. Gao, P., S. He, X. Wei, et al., "Compact printed UWB diversity slot antenna with 5.5-GHz band-notched characteristics," *IEEE Antennas Wireless Propag. Lett.*, Vol. 13, 376–379, 2014.

17. Sharawi, M. S., "Current misuses and future prospects for printed multiple-input, multiple-output antenna systems," *IEEE Antennas and Propag. Magazine*, 162–170, April 2017.

18. Ren, J., W. Hu, Y. Yin, and R. Fan, "Compact printed MIMO antenna for UWB applications," *IEEE Antennas Wireless Propag. Lett.*, Vol. 13, 1517–1520, 2014.

19. Liu, L., S. W. Cheung, and T. I. Yuk, "Compact MIMO antenna for portable devices in UWB applications," *IEEE Trans. Antennas Propag.*, No. 8, 4257–4264, August 2013.

20. Zhang, J.-Y., F. Zhang, W.-P. Tian, and Y.-L. Luo, "Acs-fed UWB-MIMO antenna with shared radiator," *Electron. Lett.*, Vol. 51, No. 7, 1301–1302, 2015.

21. Kang, L., H. Li, X. Wang, and X. Shi, "Compact offset microstrip-fed MIMO antenna for band-notched UWB applications," *IEEE Antennas Wireless Propag. Lett.*, Vol. 14, 1754–1757, 2015.

22. Tripathi, S., A. Mohan, and S. Yadav, "A compact Koch fractal UWB MIMO antenna with WLAN band-rejection," *IEEE Antennas Wireless Propag. Lett.*, Vol. 14, 1565–1568, 2015.

23. Zhu, J., B. Feng, B. Peng, L. Deng, and S. Li, "A dual notched band MIMO slot antenna system with Y-Shaped defected ground structure for UWB applications," *Microvave and Optical Technology Letters*, Vol. 58, No. 3, 626–630, March 2016.

24. Zhu, J., B. Feng, B. Peng, S. Li, and L. Deng, "Compact CPW UWB diversity slot antenna with dual band-notched characteristics," *Microwave and Optical Technology Letters*, Vol. 58, No. 4, 989–994, April 2016.

25. Kumar, J., "Compact MIMO antenna," *Microvave and Optical Technology Letters*, Vol. 58, No. 6, 1294–1298, 2016.

26. Deng, J.-Y., L.-X. Guo, and X.-L. Liu, "An ultrawideband MIMO antenna with a high isolation," *IEEE Antennas Wireless Propag. Lett.*, Vol. 15, 182–185, 2016.